PCCP

Accepted Manuscript




ROYAL SOCIETY OF CHEMISTRY

www.rsc.org/pccp

Journal Name

ARTICLE

# $BNg_3F_3$, the First Three Noble Gas Atoms Inserted Mono-centric Neutral Compounds, A Theoretical Study

Received 00th January 20xx,
Accepted 00th January 20xx

DOI: 10.1039/x0xx00000x

www.rsc.org/

Wei Chen,[a] Guang-Hui Chen,[a] Di Wu[b] and Qiang Wang[c]

Following the study of HXeOXeH and HXeCCXeH, $H_2O$ and $C_2H_2$ inserted with two Xe atoms theoretically and experimentally, the structures and stability of $BNg_3F_3$ (Ng=Ar, Kr and Xe), $BF_3$ inserted with three Ng atoms, have been explored theoretically at the DFT and *ab initio* calculations. It is shown that $D_{3h}$ symmetried $BNg_3F_3$ (Ng=Ar, Kr and Xe) are local minima with short B-Ng bond lengths at 1.966, 2.027 and 2.214 Å at the CCSD(T)/aug-cc-pVTZ/LJ18 level, which are close to their covalent limit. Note that although $BNg_3F_3$ (Ng= Kr and Xe) are energetically higher than dissociation products 3Ng + $BF_3$, they are still kinetically stable as metastable species with protecting barriers at 13.38 and 17.99 kcal/mol for $BKr_3F_3$ and $BXe_3F_3$. Moreover, $BKr_3F_3$, as tri-Kr-inserted compound, even has comparable kinetic stability with HXeOXeH and HXeOXeF. In addition, upon the formation of $BNg_3F_3$, there is large amount of charge transferred from B to Ng at least 0.619 *e*, the calculated Wiberg Bond Indices (WBI) suggest that B-Ng bonds are naturally singly bonded, the large vibrational frequencies of B-Ng and Ng-F stretching modes and negative Laplacian electron density of B-Ng bonds confirm further that $BNg_3F_3$ are stiff molecules with covalent B-Ng bonds. It should be noted that three Ng atoms inserted to mono-centric neutral molecules haven't been reported so far. We hope the present theoretical study may provide important evidence for experimental synthesis of $BNg_3F_3$.

## Introduction

Noble gas (Ng) is inert in chemistry, because of their stable octet electronic configuration in their ground state, thus, synthesis and prediction of Ng compound is always a challenge to chemists. However, after the first Ng compound, $XePtF_6$, experimentally identified in 1962 by Neil Bartlett,[1] more and more kinds of noble gas compounds have been predicted theoretically and even synthesized experimentally in recent decades, which makes chemists creative to predict and verify on noble gas chemistry field.

Recently, among the verified Ng containing compounds, the Ng inserted compounds receive extensive attentions. In the year of 1995, one-Ng-inserted compounds with the general formula of HNgX (where Ng=Ar, Kr, and Xe and X = electronegative atom or group) prepared by Räsänen and co-workers received considerable attention and expanded the field tremendously,[2-8] especially, HArF,[4] as the first argon inserted stable compound, give a great barrier of 0.35 eV (8.07 kcal/mol). This work motivates the researchers to predict and prepare various new ionic and neutral noble gas insertion compounds.[9-33] Later, Khriachtchev *et al.*[34] reported the identifications of HXeCCH ($C_{\infty v}$), HXeCC ($C_{\infty v}$), and the first two-Ng-inserted compound, i.e., HXeCCXeH ($D_{2h}$), experimentally and theoretically. And then, Yockel *et al.*[35] enriched two-Ng-inserted organic molecules by instead hydrogen to halogen, i.e. XNgCCNgX (Ng = Ar, Kr; X = F, Cl). Subsequently, Khriachtchev *et al.*[36] identified the smallest known neutral molecule with two Xe atoms inserted into $H_2O$ experimentally and theoretically, i.e., HXeOXeH ($C_{2v}$) at extremely low temperature. Following that, Avramopoulos *et al.*[37] reported one and two fluorine substitution of HXeOXeH theoretically, that is, metastable HXeOXeF ($C_s$) and FXeOXeF ($C_{2v}$), which increased the two-body decomposition barriers from 13.14 kcal/mol of HXeOXeH to 14.90 kcal/mol of HXeOXeF and 49.50 kcal/mol of FXeOXeF. All above two-Ng-atom inserted compounds give stiff structures, and even shorter bond lengths than one-Ng-inserted compound and mostly are identified by IR spectrum. Moreover, Gerber[38] predicted a slightly bent molecule, inserting with three Xe atoms in organic HCCCCH (butadiyne), HXeCCXeCCXeH, as tri-Ng-inserted compounds while which is not mono-centric insertion like HXeCCXeH. Note that all above Ng inserted compounds are based on neutral main group molecules without transition metal as central atom, with characteristic covalent bonds of H-Ng, Xe-C, and Xe-O with lengths close to their covalent radii.

[a] *Department of Chemistry, Shantou University, Shantou 515063, China. E-mail: ghchen@stu.edu.cn*
[b] *Institute of Theoretical Chemistry, Jilin University Changchun 130023, China*
[c] *Department of Applied Chemistry, College of Science, Nanjing Tech University Nanjing 211816, (China)*

Electronic Supplementary Information (ESI) available: Covalent and van der waals limits of B-Ng and Ng-F, harmonic vibrational frequencies of $F_2BNgF$, $FBNg_2F_2$ and **TS1**-**3**, geometrical parameters of transition state, IRC profiles of $BNg_3F_3 \rightarrow BF_3$+3Ng, the plotted ELF diagrams of $F_2BNgF$ and $FBNg_2F_2$ (Ng=Ar, Kr and Xe). The geometrical parameters, charge distribution, the Laplacian electron density ($\nabla^2\rho$) contour line diagram and ELF diagram of $BXe_3H_3$ ($D_{3h}$).
See DOI: 10.1039/x0xx00000x

Their achievements inspire us to find tri-Ng-atom inserted compound with mono center. $BF_3$ molecule is mostly appropriate for insertion because electronegative atom F will benefit the making of Ng-F bond. For example, one-Ng-inserted compound of $FXeBF_2$ as a white solid has been synthesized by Xe and $O_2BF_4$ under 173K on the basis of analytical and vibrational spectroscopic data,[39] and $FNgBF_2$ (Ng=Ar, Kr and Xe) were found to be thermally metastable[40] from theoretically study. Moreover, the formula of XBNgF is one of the most regular noble gas compounds, OBNgF,[41] SBNgF,[42] $NBNgF^-$,[43] $FNgBF^+$,[44] and RNBNgF[45] (Ng= Ar, Kr, Xe; R=H, $CH_3$, CCH, $CHCH_2$, F, and OH).

In this context, we try to insert three Ng (Ng=Ar, Kr and Xe) atoms into the B-F bonds of $BF_3$ to form mono-centric $BNg_3F_3$ using quantum chemical calculations. Previously, we also tried to insert three Ng atoms into $BH_3$, but abandoned them because of their long B-Xe and Xe-H bond lengths as shown in Table S1 (Support Information). From the analysis of geometrical structures, potential energy surfaces, bonding nature and harmonic frequencies, we found there exist strong B-Ng and Ng-F bonds in $BNg_3F_3$ with large kinetic stabilities.

## Computational Methods

All calculations were carried out with GAUSSIAN 09[46] and MOLCAS 8.0[47] program packages. The employed basis sets for B, F, Ar and Kr atoms are Dunning's correlation consistent triple-ζ augmented with diffuse functions (aug-cc-pVTZ).[48-50] For Xe atom, we employed LaJohn 18 valence electrons (LJ18),[51] aug-cc-pVTZ-pp,[52] and Stuttgart/Dresden (SDD)[53] basis sets together with corresponding scalar relativistic effective core potentials. LJ18 pseudopotential has been previously demonstrated to be efficient and reasonably accurate for compounds with Xe, while aug-cc-pVTZ-pp basis set and ECP can describe the electronic structure and wavefunction very well. However, the SDD pseudopotential is implemented for the consideration of cost saving of the post-HF calculations and comparison of relativistic effects.

The optimizations of $BNg_3F_3$ were performed at the hybrid-meta-exchange correlation functional (M06-2X)[54] of density functional theory (DFT), the second-order Møller–Plesset perturbation (MP2),[55] and the coupled cluster levels of theory including the contribution from single and double substitutions and an estimate of connected triples [CCSD(T)].[56,57] Herein, we use M06-2X functional rather than popular B3LYP functional, just because M06-2X has been very successful in the description of many types of chemical bonding containing Ng atoms, but B3LYP is not.[58] In addition, The multi-reference property of the optimized $BNg_3F_3$ structures is checked by calculations of diagnostic factor[59] (T1) at the CCSD(T) level. It is shown that the T1 for all $BNg_3F_3$ are 0.0305 of $BAr_3F_3$, 0.0240 of $BKr_3F_3$, and 0.0213 of $BXe_3F_3$, respectively, which are larger than 0.02. Therefore, multi-configurational method, CASSCF are performed. It's impossible that all valence electrons of $BNg_3F_3$ are considered, $BNg_3F_3$ ($D_{3h}$) were optimized at Abelian $C_{2v}$ group for saving source, actually, BNgF group on $C_2$ axis is independent with two others, and CASSCF(18,15) is chosen, because it can give almost the same bond lengths of $BNg_3F_3$ with optimization limited in $C_{2v}$ symmetry, and the active electrons are less than 0.02 *e* in the unoccupied valence space. Herein, the active space of (18, 15) was adopted, indicating that totally 18 valence electrons were activated in 15 molecular orbitals (MOs), including 9 occupied orbitals and 6 unoccupied orbitals.

Furthermore, any located critical point was verified as energy minimum or transition state (TS) by calculating their harmonic frequencies, and all transition states were unambiguously related to its interconnected energy minima by intrinsic reaction coordinate (IRC) calculations. In the energetic calculations, the zero-point vibrational energies (ZPVE) are taken into account. Note that anharmonic vibrations may have effect on the vibrational frequencies observed, and the anharmonic vibrational frequencies were derived from the vibrational self-consistent field (VSCF) and its extension by corrections via second-order perturbation theory (CC-VSCF)[60-63] using NWChem program of version 6.5.[64]

The natural population analysis (NPA) and chemical bonding analysis were carried out based on the theory of natural bond orbital in NBO 3.1 package as implemented by GAUSSIAN 09 program.[46] The chemical bonding topology analysis based on the Quantum Theory of Atoms-In-Molecule (QTAIM)[65] was used to explore the property of bond critical point (BCP), while Electron Localization Function (ELF)[66] calculation was performed to describe bonding nature by color-scale plot, as implemented in the Multiwfn 3.6 program.[67] The electron density function (EDF) information was utilized to represent the corresponding inner-core density to avoid the error that pseudopotential added on Xe. Hence, the result of the wavefunction analysis that is purely based on electron density can be almost identical to the full-electron one, but we should notice that EDF information has no effect on the real space functions that relied on wavefunction (e.g. kinetic energy density, ELF).

## Results and Discussion

To be concise, the results and discussion are organized as follows: in section A, we will give the geometrical structures of the optimized minima and transition states of $BNg_3F_3$ (Ng=Ar, Kr, Xe); in section B, the decomposition energy and stability of the obtained minima will be discussed; in section C, charge distribution and bonding of $BNg_3F_3$ will be analyzed to obtain the nature of Ng-F and B-Ng bonding; in section D, harmonic vibrational frequencies of $BNg_3F_3$ species will be assigned.

### A. Geometrical Structures of $BNg_3F_3$ (Ng=Ar, Kr and Xe)

For $BNg_3F_3$(Ng=Ar, Kr and Xe), that is, mono-centric tri-Ng-atom inserted neutral molecules, the geometrical structures of $D_{3h}$ symmetry were optimized at M06-2X, MP2, CCSD(T) and CASSCF levels, respectively, as plotted in Figure

1 and listed in Table 1. Note that all the calculated harmonic vibrational frequencies are real ones, indicating there are local minima.

The MP2, M06-2X (in parentheses) and CCSD(T) (in square brackets) calculations with aug-cc-pVTZ/LJ18 basis set gave B-Ng bond lengths at 1.878 (1.842) [1.966], 2.006 (2.004) [2.027] and 2.118 (2.209) [2.193] Å and Ng-F lengths at 1.944 (1.961) [1.998], 2.027 (2.029) [2.037] and 2.122 (2.112) [2.124] Å for Ng=Ar, Kr and Xe, respectively. Note that bond lengths at CCSD(T) level are invariably longer than those of at the other two levels. In view of the possibility of multi-configurational effect, the CASSCF(18,15) level calculations were performed and gave B-Ng at 1.796, 1.997 and 2.264 Å of and Ng-F at 1.993, 2.049 and 2.134 Å, respectively, which are generally shorter than single-slater-determinant methods except for B-Xe of $BXe_3F_3$. Note that the distance of neighboring Ar-Ar, Kr-Kr and Xe-Xe in $BNg_3F_3$ at 3.353, 3.511 and 3.849 Å are longer than those of $HNgNgF$[68] at CCSD(T)/aug-cc-pVTZ/SDD level, but which are shorter than the van de waals radii of Ng-Ng,[69] respectively, indicating that the present Ng-Ng weak interaction in $BNg_3F_3$ possibly make themselves more stable.

To test the stability of $BNg_3F_3$ geometrically, we try to add one extra $F^-$ (F1) anion to bond with boron atom of $BNg_3F_3$ ($D_{3h}$) from $C_3$ axis to form $C_{3v}$ symmetried $F_3Ng_3BF^-$ at the MP2 and M06-2X levels of theory. Take the MP2 calculations as an example, the B-Ng of the $F_3Ng_3BF^-$ (Ng=Ar, Kr and Xe) are slightly elongated to 1.902, 2.069 and 2.294 Å from $BNg_3F_3$, and those of Ng-F are elongated to 2.147, 2.199 and 2.288 Å as listed Table 2, respectively. At the same time, the Ng-Ng distances are shortened. Furthermore, all B-Ng-F in $F_3Ng_3BF^-$ still keep linear, but the ∠Ng-B-Ng reduce to 106.8°, 107.7° and 109.6° with the ∠Ng-B-F1 changed to 112.0°, 111.2° and 110.3° for Ng=Ar, Kr, and Xe, which are very close to 109.5°, indicating the covalent bond nature of B-Ng in $F_3Ng_3BF^-$ and the transformation from $sp^2$ to $sp^3$ hybrid orbital of boron atom. The successful optimization of $F_3Ng_3BF^-$ provides evidence of the probable large stability of $BNg_3F_3$, since the additional $F^-$ did not give rise to great geometrical changes of $BNg_3F_3$ and just get a rational symmetrical change according to hybrid orbital theory.

Furthermore, we also tried to optimize the compounds with one or two Ng atoms inserted into $BF_3$, i.e., $F_2BNgF$ and $FBNg_2F_2$ (Ng=Ar, Kr and Xe), and found that they are both local minima with real frequencies as plotted in Figure 1 and summarized in Table 1. At the MP2/aug-cc-pVTZ/SDD level, the calculated Ng-F (Ng=Ar, Kr and Xe) are 2.075, 2.098, and 2.172 Å in sequence for $F_2BNgF$ as well as 1.991, 2.052, and 2.153 Å for two-Ng-inserted $FBNg_2F_2$ ($C_{2v}$), which are longer than that of 1.944, 2.026 and 2.137 Å for $BNg_3F_3$, respectively. But the B-Ar bond lengths of $F_2BArF$, $FBAr_2F_2$ and $BAr_3F_3$ increase slightly from 1.835 to 1.863 and 1.878 Å, which is different from the almost equal lengths of B-Kr and B-Xe bonds in $F_2BNgF$, $FBNg_2F_2$ and $BNg_3F_3$, which are almost with equal lengths at MP2/aug-cc-pVTZ/SDD level. Thus, one, two or three inserted Ng atoms including Ar, Kr and Xe certainly cannot elongate the Ng-F and B-Ng bonds greatly in $BF_3$.

It is of interest to compare the B-Ng and Ng-F bond lengths with some Ng inserted analogs, such as linear $FNgBF^+$,[44] $FNgBN^-$,[43] and $FNgBNH$[45] (Ng=Ar, Kr and Xe). It was found that the B-Ng bond lengths in $FNgBF^+$ (Ng=Kr and Xe) with 2.186 and 2.311 Å, and those of Ng-F in $FNgBN^-$ (Ng=Ar, Kr and Xe) with 2.293, 2.311 and 2.349 Å are longer than those of $BNg_3F_3$ at CCSD(T)/aug-cc-pVTZ/SDD level. But the 1.873 and 1.966 Å of Ng-F in $FNgBF^+$ (Ng=Kr and Xe) are slightly shorter than that in $BNg_3F_3$. Therefore, $BNg_3F_3$ give reasonable bond lengths compared with $FNgBF^+$, $FNgBN^-$.

**B. Decomposition energies and stabilities of $BNg_3F_3$ (Ng=Ar, Kr, and Xe)**

To ascertain the stability of $BNg_3F_3$ species, the reaction potential energy surfaces (PESs) of decomposition have to be built as plotted in Figure 2. It has been shown that the DFT method often yields for noble-gas hydrides more reliable energetics than the MP2 method.[70] Moreover, M06-2X functional performed very well on the B-Ng bond distance with mean unsigned errors less than 0.02 Å in most cases.[58] Thus, the related compounds of $BNg_3F_3$ as well as various possible decomposed products are optimized at the M06-2X/aug-cc-pVTZ/LJ18 and refined at the single-point CCSD(T)/aug-cc-pVTZ/LJ18 levels, simplified as CCSD(T)//M06-2X in Table 4. For all the three $D_{3h}$ symmetried $BNg_3F_3$ (Ng=Ar, Kr and Xe) species, the possible decomposition channels fall into three groups, i.e., (1) ~ (5) correspond to molecular and atomic channels; (6) ~ (8) correspond to ionic channels; and channel (9) ~ (11) correspond to stable species theoretically reported, including $F_2$, $NgF_2$ (Ng=Kr and Xe), and $FNgNgF$,[71] respectively. The first group is listed as follows:

$$BNg_3F_3 \rightarrow FBNg_2F_2 + Ng \rightarrow F_2BNgF + 2Ng \rightarrow BF_3 + 3Ng \quad (1)$$

$$\rightarrow B + 3Ng + 3F \text{ or } B + 3Ng + F_2 \quad (2)$$

$$\rightarrow BNg_2F_2 + Ng + F \text{ or } BNg_2F_2 + NgF \quad (3)$$

$$\rightarrow BNgF\ (^1\Sigma) + 2Ng + 2F \text{ or } BNgF\ (^1\Sigma) + 2NgF \quad (4)$$

$$\rightarrow BNgF\ (^3\Pi) + 2Ng + 2F \text{ or } BNgF\ (^3\Pi) + 2NgF \quad (5)$$

Channel (1) corresponding to the decomposition to the global minimum ($BF_3$+3Ng) is preceeding in three steps with respective transition states (**TSs**) as plotted PES in Figure S1 and the detailed IRC profiles are plotted in Figure S2. At first, one Ng-F bonds are elongated with relevant B-Ng bond shortened, the fluorine atom breaks away from the plane to form **TS1** with 5.70, 13.38, and 17.99 kcal/mol to $FBNg_2F_2$+Ng as plotted in Figure S1 followed by, $FBNg_2F_2$ decomposed to $F_2BNgF$+Ng via **TS2** by 9.72, 15.70 and 21.67 kcal/mol, respectively. Note that the $C_{2v}$ symmetried $FBNg_2F_2$ and $F_2BNgF$ are plotted in Figure 1. At last, $F_2BNgF$ decompose to $BF_3$+Ng via **TS3** with 7.14, 15.03 and 24.98 kcal/mol for Ng=Ar, Kr and Xe, respectively. Note that **TS3** has been reported by Ghanty.[15] It is found that the process

from $BNg_3F_3$ to $BF_3$ + 3Ng are exothermic largely by ca. 323.47~498.79 kcal/mol. Probably, it may be a record-breaking value for high-energy materials. Note that the two-body decomposition reaction of $BNg_3F_3$ (Ng=Kr and Xe) have transition states that are higher than that of two-Ng-inserted compound, including experimentally verified HXeOXeH at 13.14 kcal/mol,[36] as well as HXeOXeF[37] and HXeXeF[68] at 14.90 and 11.76 kcal/mol, but lower than that of FXeOXeF[37] and HXeCCXeH[34] at 62.26 and 49.50 kcal/mol.

Note that except for channel (1), all the total energies of decomposition fragments in (2)~(11) are energetically higher than $BNg_3F_3$ for Ng = Kr and Xe, so we need not search for any transition states in view of the thermodynamic stability of $BNg_3F_3$ (Ng = Kr and Xe). Just like the decomposition of Ng inserted molecules $(HNgY)^{2-8}$ to atoms of H + Ng + Y, the channel (2) of $BNg_3F_3$ dissociating to B + 3Ng + 3F are endothermic largely by 30.24 and 134.14 kcal/mol for Ng = Kr and Xe, while exothermic by 40.11 kcal/mol for $BAr_3F_3$. Channel (3) related to a radical precursor of $BNg_2F_2$, whose reverse reaction probably leads to $BNg_3F_3$, just similar to the reaction of H + Xe + OXeH leading to HXeOXeH.[36] Thus, exothermicity of 3.39 and 53.74 kcal/mol for $BKr_3F_3$ and $BXe_3F_3$ may be obtained experimentally easier than the endothermicity of 27.86 kcal/mol for $BAr_3F_3$ in channel (3). Unlike one or two Ng atoms inserted compounds, tri-Ng-atom inserted compounds may have more precursors. Channel (4) and (5) are related to the possible radical precursors, i.e., BNgF can be in singlet or triplet states with the former more stable energetically with the calculated S-T gap at 6.82, 21.44 and 34.66 kcal/mol, respectively. Note that BNgF ($^3\Pi$) radical in channel (5) with two unpaired electrons can be deemed to be precursor of $BNg_3F_3$, which can react with 2NgF to produce $BKr_3F_3$ and $BXe_3F_3$ with exothermicity of 23.89, 115.34 kcal/mol, but for BArF ($^3\Pi$) it is an endothermic process of 46.90 kcal/mol to produce $BAr_3F_3$. It should be noted that XeF radical is calculated to be energetically below Xe + F largely by 12.66 kcal/mol while ArF and KrF are just 0.10 and 0.98 kcal/mol below Ar + F and Kr + F, respectively. Accordingly, XeF, as a reactant of reverse reaction of channel (3), (4) and (5), can reduce the number of reactant and thus increase the probability of effective collision.

$$BNg_3F_3 \rightarrow 3F^- + B^{3+} + 3Ng \quad (6)$$

$$\rightarrow 3NgF^+ + B^{3-} \quad (7)$$

$$\rightarrow BNg_3^{3+} + 3F^- \quad (8)$$

Channel (6) ~ (8) corresponding to the decomposition of $BNg_3F_3$ by channel (6) and (7) are endothermic in the range of 1057.92~1544.57 kcal/mol. The large decomposition energies of channel (8) to $BNg_3^{3+}$ and $3F^-$ from 762.18 to 753.01 and 725.90 kcal/mol reveal $BNg_3F_3$ are not van der waals complexes, and fluorine plays a vital role on the stability of $BNg_3F_3$. Therefore, there is large thermodynamic stability of $BNg_3F_3$ towards ionic decompositions. The species in channel (8) can be best described by the Lewis structures of $(BNg_3^{3+})(F^-)_3$, with the B-Ng bonds in $BNg_3^{3+}$ at 1.781, 1.944 and 2.144 Å at CCSD(T)/aug-cc-pVTZ/LJ18 level, which are shorter than that in $BNg_3F_3$ just like the shorter H-Ng bond of $HNg^+$ (Ng= He, Ar, Kr and Xe) than that in HNgF.

$$BNg_3F_3 \rightarrow BNg^+(^1S) + F^- + 2Ng + F_2$$
$$\text{or } BNg^+(^3P) + F^- + 2Ng + F_2 \quad (9)$$

$$\rightarrow BNg^+(^1S) + F^- + FNgNgF$$
$$\text{or } BNg^+(^3P) + F^- + FNgNgF \quad (10)$$

$$\rightarrow BNg^+(^1S) + F^- + NgF_2 + Ng$$
$$\text{or } BNg^+(^3P) + F^- + NgF_2 + Ng \quad (11)$$

Note that $F^-$ and $BNg^+$ (Ng=Ar, Kr and Xe) with two electronic configurations ($^1S$ and $^3P$) are involved in channel (9)~(11). The endothermic processes of channel (9) [26.53~181.01 kcal/mol for $BNg^+$ ($^1S$) and 103.19~238.87 kcal/mol for $BNg^+$ ($^3P$)] indicate large thermodynamically stability of $BNg_3F_3$ in the presence of $F_2$. The similar endothermic process of channel (10) involves the reported species of FNgNgF[71] with short Ng-Ng bond and large kinetic stability. In channel (11) there are experimentally found molecules of $NgF_2$ (Ng=Kr, Xe), note that all $NgF_2$ (Ng=Ar-Xe) can be optimized at the M06-2X, MP2 and CCSD(T) levels, but there is an abnormal increase of Ar-F distance to 2.941 Å at CCSD(T) level compared with that of 1.756 and 1.862 Å at M06-2X and MP2 levels. Actually, $ArF_2$ was predicted to be unstable with negative three-body decomposition energies at CCSD(T)/CBS level[45] and has still not been synthesized. This reveals the more reliable calculations of CCSD(T) than that of M06-2X and MP2.

It is important to compare the thermodynamic and kinetic stabilities upon the insertion of Ng (Ng= Ar, Kr and Xe) atom into $BF_3$ gradually. From channel (1), it is clear that $FBAr_2F_2$ and $FBKr_2F_2$ are kinetically the most stable species of $BNg_nF_3$ (Ng=Ar and Kr, n=1, 2 and 3) with respective barriers at 9.72 and 15.70 kcal/mol, while $F_2BXeF$ are kinetically more stable than $FBXe_2F_2$ and $BXe_3F_3$. Among $BNg_3F_3$, $BKr_3F_3$ and $BXe_3F_3$ are energetically higher than $BF_3$ + 3Ng and thus thermodynamically unstable in channel (1), however, they are kinetically stable in the decomposition via **TS1** with 13.38 and 17.99 kcal/mol, respectively, but $BAr_3F_3$ is both thermodynamically unstable in molecular and atomic channels (1) ~ (5) and kinetically unstable in channel (1) with a small barrier of 5.70 kcal/mol. Therefore, $BKr_3F_3$ and $BXe_3F_3$ are kinetically stable as metastable species. Note that even $BKr_3F_3$ has a large protecting barrier close to two-Ng-inserted HXeOXeH and HXeOXeF.[36,37] Thus, in view of the successful synthesis of analogous $F_2BXeF$ by Xe and $O_2BF_4$ under 173K,[39] both $BKr_3F_3$ and $BXe_3F_3$ may be prepared in low-temperature noble-gas matrixes using UV photolysis of a $BF_3$ precursor and subsequent thermal mobilization of B atoms.

### C. Charge distribution and bonding nature

To explore the bonding nature of $BNg_3F_3$, we also calculated the charge distribution, WBIs, QTAIM,[65] and ELF.[66] From the calculated NPA charge of $BNg_3F_3$ species at the MP2/aug-cc-pVTZ/SDD level, it is found that the charge on the B atom ($q$B) changes from 1.570 ($BF_3$) to 0.641, 0.245 and -0.267 *e* in $BAr_3F_3$, $BKr_3F_3$ and $BXe_3F_3$ respectively, as summarized in

Table 3, while those of F atom keep negative from -0.523 ($BF_3$) to -0.832, -0.826 and -0.844 *e*, due to its large electronegativity. Accordingly, the inserted Ng atom generally loses electron with positive charge at 0.619, 0.745 and 0.923 *e* for Ar, Kr and Xe, indicating the breaking of their closed-shell structures, and the participation to the chemical bonds with the neighboring B and F atoms.

Now, it is of interest to compare the difference of NPA charge between $BNg_3F_3$ and $F_3Ng_3BF^-$ as listed in Table 3. It is found that the charge (*q*F1) of the added $F^-$ on $C_{3v}$ axis are -0.518, -0.550 and -0.591 *e* for Ng= Ar, Kr and Xe in $F_3Ng_3BF^-$, which means $BNg_3F_3$ group in $F_3Ng_3BF^-$ acquire -0.482, -0.450 and -0.409 *e* from F1 anion, respectively. At the same time, the remaining *q*F of $F_3Ng_3BF^-$ increases to -0.937, -0.919 and -0.911 *e*, and *q*B increases to 0.835, 0.541 and 0.171 *e*, leading to more electrons on Ng atoms and thus with fewer positive charges than original $BNg_3F_3$ (Ng=Ar, Kr and Xe).

The calculated Wiberg bond indices (WBIs) of for B-Ng bonds are 0.879, 0.945 to 1.037 in $BAr_3F_3$, $BKr_3F_3$ and $BXe_3F_3$, suggesting singly bonded B-Ng as listed in Table 5. At the same time, the small WBIs of 0.147, 0.166, and 0.168 for Ar-F, Kr-F and Xe-F suggest that essentially weak Ng-F interactions. Note that the analogous $D_{3h}$ symmetried anion with three Ng atoms, i.e., $(NgO)_3F^-$ (Ng=He, Ar, and Kr) reported by Hu *et al*.[72] indicate that the interaction between $F^-$ and NgO are non-covalent with the large Ng-F bond lengths.

Following the works of Gerry and co-workers[73-75] about the covalent and van der Waals limits, we conclude the covalent and van der Waals limits of B-Ng and Ng-F bond[76-79] by comparing B-Ng and Ng-F bond lengths of $F_2BNgF$, $FBNg_2F_2$, and $BNg_3F_3$ as listed in Table S3. Note that r(B-Ng) is closest of all to the covalent limit and much less than the van der Waals limit. Although r(Ng-F) exceeds the covalent limit (by ~0.452Å), it is still much less than the van der Waals limit. Therefore, B-Ng bonds are the covalent nature from the view of bond lengths.

The quantum chemistry theory of atoms-in-molecule, QTAIM,[65] is known as a powerful and universal utility in investigating the bond critical point (BCP) properties of unusual Ng bonding. In Table 4, we listed the detailed QTAIM information of BCP for $F_2BNgF$, $FBNg_2F_2$ and $BNg_3F_3$ (Ng=Ar, Kr and Xe) including electron density (ρ), Laplacian electron density ($\nabla^2\rho$) (contour line diagrams in Figure 4), energy density ($H_r$), potential energy density ($V_r$) and kinetic energy density ($G_r$). From Table 1, it is clear that the B-Ng bond distances of $BNg_3F_3$ are close to their $R_{cov}$ of 1.81, 2.02 and 2.16 Å,[80] but Ng-F bond distances much longer than corresponding $R_{cov}$ 1.68, 1.81 and 2.01 Å.[80] Thus, the best discussion of the study by Boggs[81] can be performed, i.e., the chemical bonds can be defined to meet any criteria of the following four bond types including A, B, C, and $W^c$:

- Type A. $\nabla^2\rho(r) < 0$, and ρ(r) is large (with a threshold of 0.1 au);
- Type B. H(r) < 0, and ρ(r) is large (with a threshold of 0.1 au);
- Type C. H(r) < 0 and G(r)/ρ(r)<1;
- $W^c$. H(r)< 0 and G(r)/ρ(r)> 1;

In general, type A can be looked on as a subset of type B and/or C, whereas H(r) < 0 and G(r)/ρ(r)<1 indicating that the bonding is of partially covalent in nature under the category of type C covalent bond. B-Ng interactions could be classified as covalent bonds of type A, B and C, except for B-Ar in $F_2BArF$ of type B and C because of its positive Laplacian electron density on BCP. In addition, the B-Ng bond property on BCP both reveals the local charge concentration area as displayed in Figure 4. However, the Ng-F interactions could be in principle classified as weak bonding interaction with some covalent properties due to there are H(r)< 0 and G(r)/ρ> 1 ($W^c$) with the positive values of $\nabla^2\rho(r)$. Obviously, the strength of B-Ng is consistent to area of $\nabla^2\rho(r) < 0$, that is B-Ar < B-Kr < B-Xe, which is also in agreement with the calculated Wiberg bond indices of 0.879, 0.945 and 1.037 for B-Ar, B-Kr, and B-Xe.

In addition, we also compared the bonding nature of $F_2BNgF$, $FBNg_2F_2$ and $BNg_3F_3$ (Ng=Ar, Kr and Xe) with QTAIM[65] at MP2/aug-cc-pVTZ/LJ18 level as listed in Table 5. It is shown that the B-Ar bond has increasing covalent composition from $F_2BArF$ to $FBAr_2F_2$ and $BAr_3F_3$, according to Laplacian electron density [$\nabla^2\rho(r)$] of +0.030, -0.144 and -0.154, and corresponding electron density [ρ(r)] increased from 0.123 to 0.130 and 0.146. At the same time, the B-Ar covalent bond changes from types B and C to types A, B and C. Correspondingly, the Ar-F bond, as a $W^c$ interaction, the increased positive Laplacian electron density and electron density on BCP reveal the enhance of this interaction with increasing number of inserted Ng atom, and reliably, the increased WBI of Ar-F bonds from 0.082 to 0.121 and 0.147 of $F_2BArF$, $FBAr_2F_2$ and $BAr_3F_3$. Hence, more inserted Ar or Kr atoms will benefit the strength of B-Ar and Ar-F as well as B-Kr and Kr-F bonds. But this effect isn't distinct, and more Xe atoms inserted to $BF_3$ will make B-Xe and Xe-F bonds weaker from the QTAIM data that the electron density of BCP in B-Xe bond changes from 0.129 in $F_2BXeF$ to 0.125 in $FBXe_2F_2$, and to 0.126 in $BXe_3F_3$. Although the strength of B-Xe was not increased with the increasing number of inserted Ng atoms, it is no doubt that B-Xe are all covalent bonding in $F_2BXeF$, $FBXe_2F_2$, and $BXe_3F_3$ due to the negative Laplacian electron density.

To confirm the above analysis of bonding nature, we also calculated the Electron Localized Function (ELF).[66] Generally, ELF diagram can provide a faithful visualization of valence shell electron pair repulsion theory (VSEPR).[82] As the plotted ELF diagrams of $BNg_3F_3$, $FBNg_2F_2$, and $F_2BNgF_3$ in Figure 5 and S1, note that the red areas with the largest ELF values (yellow area) between Ng and B atoms denote the low local kinetic energy densities owing to relatively low Pauli repulsion, indicating the covalent interactions of B-Ng bonding. On the other hand, the yellow area doesn't appear between Ng and F, F basins are relatively independent, which indicates that Ng-F bonding are rather ionic, or non-covalent. After careful analysis, it is shown that the low-ELF areas between Ng and F atoms are of increasing covalent bond tendency of Ng-F bonds from Ar to Kr and Xe.

Now, it's interesting to compare the B-Ng bonding with that in other noble gas compounds, such as the B-Ng bonding in $BNg_3F_3$, B-Ng bonds in OBNgF,[41] FNgBS[42], $FNgBN^-$,[43] and FBNgNH[45] (Ng=Ar, Kr, Xe) are dominant in covalent character from the negative Laplacian electron density of BCP, but the BCP values of B-Ng bond in $HNgBF^+$ (Ng=He, Ar, Kr, Xe)[83] indicate that ion-dipole interaction play a major role in the B-Ng bonding with a strong ionic character.

Note that the B-Ng bonds are covalent and Ng-F bonds are $W^c$ interaction in $BNg_3F_3$, which is totally different from the bonding nature of HXeOXeH, where the corresponding O-Xe bonds are mostly ionic with a substantial covalent contribution while Xe-H bond is predominantly covalent. This can be rationalized from the analysis of atomic electronegativity, i.e., the electronegativity of 3.44 for O, 3.98 for F are much larger than that of Ng, while those of 2.20 for H, 2.04 for B are close to that of Ng atoms from Pauling electronegativity scale.[84] The calculated QTAIM[65] data for $BXe_3H_3$ well confirm the above points as listed in Table 4, clearly showing that H-Xe bond is covalent from negative $\nabla^2\rho$, -0.0214, and relatively ionic of B-Xe with $\nabla^2\rho$ of -0.0072, more apparently from WBI, H-Xe bond is 0.515 as half bonded, and B-Xe bond is very weak just at 0.025. The Laplacian electron density and ELF[66] diagrams of $BXe_3H_3$ as plotted in Figure S2 and S3 (Support Information) are consistent with the QTAIM results.

### D. Vibrational frequencies

The calculated harmonic vibrational frequencies and intensities for $F_2BNgF$, $FBNg_2F_2$, and $BNg_3F_3$ are listed in Table 6 and S4, respectively. It is shown that the calculated frequencies at M06-2X and MP2 levels are in reasonable agreement, and herein we just take the MP2 calculations as an example. It is found that the harmonic frequencies of $\nu$(B-Ng) of one-Ng-inserted $F_2BNgF$ are generally smaller than that of two or three Ng-inserted $FBNg_2F_2$ and $BNg_3F_3$. This is consistent with that the B-Ng bond lengths of $BNg_3F_3$ and $FBNg_2F_2$ are generally shorter than that of $F_2BNgF$, and further confirm that the covalent character of B-Ng bond in $BNg_3F_3$ and $FBNg_2F_2$ are relatively higher than those of in $F_2BNgF$.

For $BNg_3F_3$, there are totally fifteen vibration modes including six stretching, five bending and four torsions (including an out-of-plane mode). Note that the vibrational frequencies of TS1-TS3 are also calculated as listed in Table S5-S7 (Support Information). There are five degenerated modes including δ(Ng-B-Ng), F-Ng-Ng-F torsion, δ(B-Ng-F), $\nu_{as}$(Ng-F) and $\nu_{as}$(B-Ng) due to the high $D_{3h}$ symmetry of $BNg_3F_3$. The frequencies of $\nu_{as}$(Ng-F) of $BNg_3F_3$ (Ng=Ar, Kr and Xe) modes located at high frequencies zones are larger than 400 $cm^{-1}$, i.e., 445.0, 443.2 and 439.8 $cm^{-1}$ corresponding to large intensities of 796.60, 564.97 and 517.70 km/mol, which should be the characteristic peaks for the experimental observation. But note that the experimentally observed frequencies for HArF,[4] and HXeOXeH[36] suggest that the theoretical values for the vibrational frequencies are larger by about 10 %,[85] because anharmonic effects can't be ignored. Here, we calculated the anharmonic vibrational frequencies of $BNg_3F_3$ by MP2/CC-VSCF method[60-63] as listed in Table 6. The frequencies of the characteristic peak, $\nu_{as}$(Ng-F), decrease to 435.2, 394.0 and 382.5 $cm^{-1}$, which certified the large influence of anharmonic effect for $BNg_3F_3$.

The intense stretching vibrations of $\nu$(B-Ng) and $\nu_{as}$(Ng-F) further confirm that the Ng inserted compounds based on $BF_3$ including $F_2BNgF$, $FBNg_2F_2$ and $BNg_3F_3$ are stiff and not van der waals molecules.

## Conclusion

Following the study of HXeOXeH[36] and HXeCCXeH,[34] that is, $H_2O$ and $C_2H_2$ inserted with two Ng atoms experimentally and theoretically. the species of tri-Ng-atom inserted in $BF_3$, i.e., neutral mono-centric compounds ($BNg_3F_3$, Ng=Ar, Kr, Xe), is firstly investigated at the DFT/M06-2X and *ab initio* calculations within the framework of MP2, CCSD(T) and CASSCF levels of theory. It is shown that $BNg_3F_3$ (Ng=Ar, Kr and Xe) are all identified as local minima with $D_{3h}$ symmetry with B-Ng bonds lengths at 1.966, 2.027 and 2.214 Å at the CCSD(T)/aug-cc-pVTZ/LJ18 level, which are close to their covalent radii. Moreover, when an $F^-$ ion (F1) is added on boron atom in $BNg_3F_3$, the geometries of $F_3Ng_3BF^-$ are still very tight. From the plotted PESs, it is found that $BNg_3F_3$ (Ng=Kr and Xe) are metastable species with large kinetic stability towards $BF_3$ + 3Ng with decomposition barriers of 13.38 and 17.99 kcal/mol, respectively, while that of $BAr_3F_3$ is just 5.70 kcal/mol and cannot be identified as metastable status. Specially, $BKr_3F_3$, as tri-Kr-inserted compound, even has large dissociation barrier comparable with two-Xe-inserted HXeOXeH and HXeOXeF.[37] From the bonding nature analysis, it is found that B-Ng in $BNg_3F_3$ are mainly singly covalent bond supported by negative Laplacian electron density of BCP with WBI at 0.879, 0.945 and 1.037 for Ng=Ar, Kr and Xe, while Ng-F are dominantly weak bonding interaction with some covalent properties according to Boggs's[79] criteria. Finally, the calculated anharmonic vibrational frequencies reveal that $BNg_3F_3$ are stiff molecules with the characteristic asymmetric stretching at 435.0, 394.0 and 382.5 $cm^{-1}$ for Ar-F, Kr-F and Xe-F bonds, respectively. The large kinetic stabilities of the $BKr_3F_3$ and $BXe_3F_3$ molecules suggest that they should be very likely candidates for experimental detection. Following the synthesis of one-Ng-inserted $FXeBF_2$ and two-Ng-inserted HXeOXeH, we hope that the present theoretical study may provide important evidence for experimental synthesis of $BNg_3F_3$ such as matrix photochemistry at low temperature in future.

## Acknowledgment

This work was supported by the National Natural Science Foundations of China (Nos. 21173095, 10621203094, and 21373112). In addition, we owe a debt of gratitude to Miss Min-min Ma's help in polishing the English.

## Reference


1 N. Bartlett, *Proc. Chem. Soc*., 1962, 218.

2 M. Pettersson, J. Lundell and M. Räsänen, *J. Chem. Phys.*, 1995, **102**, 6423-6431.

3 M. Pettersson, J. Lundell and M. Räsänen, *J. Chem. Phys.*, 1995, **103**, 205-210.

4 L. Khriachtchev, M. Pettersson, N. Runeberg, J. Lundell and M. Räsänen, *Nature (London)*, 2000, **406**, 874-876.

5 M. Pettersson, J. Lundell, L. Khriachtchev and M. Räsänen, *J. Chem. Phys.*, 1998, **109**, 618-625.

6 M. Pettersson, J. Lundell, L. Khriachtchev, E. Isoniemi, and M. Räsänen, *J. Am. Chem. Soc.*, 1998, **120**, 7979-7980.

7 E. Isoniemi, M. Pettersson, L. Khriachtchev, J. Lundell and M. Räsänen, *J. Phys. Chem. A*, 1999, **103**, 679-685.

8 M. Pettersson, L. Khriachtchev, J. Lundell and M. Räsänen. *J. Am. Chem. Soc.*, 1999, **121**, 11904-11905.

9 G. Liu, Y. Yang and W. Zhang, *Struct. Chem.,* 2010, **21**, 197-202.

10 A. Cohen, J. Lundell and R. B. Gerber, *J. Chem. Phys.*, 2003, **119**, 6415-6417.

11 B. R. Wilson, K. Shi and A. K. Wilson, *Chem. Phys. Lett.*, 2012, **537**, 6-10.

12 T. Jayasekharan and T. K. Ghanty, *J. Chem. Phys.,* 2008, **128**, 144314.

13 C. Y. Peng, C. Y. Yang, Y. L. Sun and W. P. Hu, *J. Chem. Phys*., 2012, **137**, 194303.

14 S. Pan, A. Gupta, S. Mandal, D. Moreno, G, Merino and P. K. Chattaraj, *Phys. Chem. Chem. Phys*., 2015, **17**, 972-982.

15 T. H. Li, C. H. Mou, H. R. Chen and W. P. Hu, *J. Am. Chem. Soc*., 2005, **127**, 9241-9245.

16 S. Borocci, N. Bronzolino and F. Grandinetti, *Chem. Phys. Lett.* 2008, **458**, 48-53.

17 S. Borocci, M. Giordani and F. Grandinetti, *J. Phys. Chem. A*, 2014, **118**, 3326-3334.

18 T. Jayasekharan and T. K. Ghanty, *J. Chem. Phys.,* 2007, **127**, 114314.

19 M. Gronowski, M. Turowski and R. Kołos, *J. Phys. Chem. A*, 2015, **119**, 2672-2682.

20 L. Khriachtchev, A. Lignell, H. Tanskanen, J. Lundell, H. Kiljunen and M. Räsänen, *J. Phys. Chem. A*, 2006, **110**, 11876-11885.

21 K. Gao and L. Sheng, *J. Chem. Phys.*, 2015, **142**, 144301.

22 A. Sirohiwal, D. Manna, A. Ghosh, T. Jayasekharan and T. K. Ghanty, *J. Phys. Chem. A* 2013, **117**, 10772−10782

23 H. Tanskanen, L. Khriachtchev, J. Lundell, H. Kiljunen and M. Räsänen, *J. Am. Chem. Soc.*, 2003, **125**, 16361-16366.

24 L. Khriachtchev, A. Domanskaya, J. Lundell, A. Akimov, M. Räsänen and E. Misochko, *J. Phys. Chem. A*, 2010, **114**, 4181–4187.

25 A. Ghosh, D. Manna and T. K. Ghanty, *J. Chem. Phys.*, 2013, **138**, 194308.

26 T. Takayanagi, T. Asakura, K. Takahashi, Y. Taketsugu, T. Taketsugu and T. Noro, *Chem. Phys. Lett.,* 2007, **446**, 14-19.

27 M. Pettersson, L. Khriachtchev, J. Lundell and M. Räsänen, *J. Am. Chem. Soc.*, 1999**, 121***,* 11904-11905

28 M. Pettersson, J. Lundell, L. Khriachtchev, E. Isoniemi and M. Räsänen. *J. Am. Chem. Soc*., 1998**, 120***,* 7979-7980

29 M. Zhang and L. Sheng, *J. Chem. Phys.*, 2013, **138**, 114301.

30 T. Jayasekharan and T. K. Ghanty, *J. Chem. Phys.*, 2012, **136**, 164312.

31 M. Zhang and L. Sheng, *Phys. Chem. Chem. Phys.*, 2014, **16**, 196-203.

32 D. Manna, A. Ghosh and T. K. Ghanty, *Chem. Eur. J.* 2015, **21**, 8290-8296.

33 A. Ghosh, D. Manna and T. K. Ghanty, *J. Phys. Chem. A*, 2014, **119**, 2233-2243.

34 L. Khriachtchev, H. Tanskanen, J. Lundell, M. Pettersson, H. Kiljunen and M. Räsänen, *J. Am. Chem. Soc.*, 2003, **125**, 4696-4697.

35 S. Yockel, E. Gawlik and A. K. Wilson, *J. Phys. Chem. A*, 2007, **111**, 11261-11268.

36 L. Khriachtchev, K. Isokoski, A. Cohen, M. Räsänen and R. B. Gerber, *J. Am. Chem. Soc.*, 2008, **130**, 6114-6118.

37 A. Avramopoulos, J. Li, N. Holzmann, G. Frenking and M. G. Papadopoulos, *J. Phys. Chem. A*, **2011**, 115, 10226-10236.

38 J. Lundell, A. Cohen and R. B. Gerber, *J. Phys. Chem. A*, 2002, **106**, 11950-11955.

39 C. T. Goetschel and K. R. Loos, *J. Am. Chem. Soc*, 1972, **94**, 3018-3021.

40 T. Jayasekharan and T. K. Ghanty, *J. Chem. Phys.*, 2006, **125**, 234106.

41 T. Y. Lin, J. B. Hsu and W. P. Hu, *Chem. Phys. Lett.*, 2005, **402**, 514-518.

42 A. Ghosh, S. Dey, D. Manna and T. K. Ghanty, *J. Phys. Chem. A*, 2015, **119**, 5732-5741.

43 P, Antoniotti, S. Borocci, N. Bronzolino, P. Cecchi and F. Grandinetti, *J. Phys. Chem. A*, 2007, **111**, 10144-10151.

44 Z. Lv, G. H. Chen, D. Li, D. Wu, X. C. Huang, Z. R. Li and W. G. Liu, *J. Chem. Phys.*, 2011, **134**, 154302.

45 J. L. Chen, C. Y. Yang, H. J. Lin and W. P. Hu, *Phys. Chem. Chem. Phys.*, 2013, **15**, 9701-9709.

46 M. J. Frisch, G. W. Trucks, H. B. Schlegel, G. E. Scuseria, M. A. Robb, J. R. Cheeseman, G. Scalmani, V. Barone, B. Mennucci, G. A. Petersson, H. Nakatsuji, M. Caricato, X, Li, H. P. Hratchian, A. F. Izmaylov, J. Bloino, G. Zheng, J. L. Sonnenberg, M. Hada, M. Ehara, K. Toyota, R. Fukuda, J. Hasegawa, M. Ishida, T. Nakajima, Y. Honda, O. Kitao, H. Nakai, T. Vreven, J. A. Jr. Montgomery, J. E. Peralta, F. Ogliaro, M. Bearpark, J. J. Heyd, E. Brothers, K. N. Kudin, V. N. Staroverov, R. Kobayashi, J. Normand, K. Raghavachari, A. Rendell, J. C. Burant, S. S. Iyengar, J. Tomasi, M. Cossi, N. Rega, J. M. Millam, M. Klene, J. E. Knox, J. B. Cross, V. Bakken, C. Adamo, J. Jaramillo, R. Gomperts, R. E. Stratmann, O. Yazyev, A. J. Austin, R.

1 Cammi, C. Pomelli, J. W. Ochterski, R. L. Martin, K. Morokuma, V. G. Zakrzewski, G. A. Voth, P. Salvador, J. J. Dannenberg, S. Dapprich, A. D. Daniels, O. Farkas, J. B. Foresman, J. V. Ortiz, J. Cioslowski and D. J. Fox, *GAUSSIAN09, Revision A02*, Gaussian, Inc., Wallingford, CT, 2009.

7 G. Karlström, R. Lindh, P. Å. Malmqvist, B. O. Roos, U. Ryde, V. Veryazov and L. Seijo, *Comput. Mater. Sci.* 2003, **28**, 222-239.

8 R. A. Kendall, T. H. Jr. Dunning and R. J. Harrison, *J. Chem. Phys*., 1992, **96**, 6796-6806.

9 D. E. Woon and T. H. Jr. Dunning, *J. Chem. Phys.*, 1993, **98**, 1358-1371.

10 A. K. Wilson, D. E. Woon, K. A. Peterson and T. H. Jr. Dunning, *J. Chem. Phys.*, 1999, **110**, 7667-7676.

11 L. A. LaJohn, P. A. Christiansen, R. B. Ross, T. Atashroo and W. C. Ermler, *J. Chem. Phys*., 1987, **87**, 2812-2824.

12 K. A. Peterson, D. Figgen, E. Goll, H. Stoll and M. Dolg, *J. Chem. Phys*., 2003, **119**, 11113-11123.

13 A. Nicklass, M. Dolg, H. Stoll and H. Preuss, *J. Chem. Phys.*, 1995, **102**, 8942-8952.

14 Y. Zhao and D. G. Truhlar, *Theor. Chem. Acc*., 2008, **120**, 215.

15 M. J. Frisch, M. Head-Gordon and J. A. Pople, *Chem. Phys. Lett.*, 1990, **166**, 275-280.

16 K. Raghavachari, G. W. Trucks and J. A. Pople, *Chem. Phys. Lett*., 1989, **157**, 479.

17 G. E. Scuseria, *Chem. Phys. Lett*., 1991, **176**, 27-35.

18 T. Y. Lai, C. Y. Yang, H. J. Lin, C. Y. Yang and W. P. Hu, *J. Chem. Phys*., 2011, **134**, 244110.

19 T. J. Lee and P. R. Taylor, *Int. J. Quantum Chem.*, 1989, **36**, 199-207.

20 J. O. Jung and R. B. Gerber, *J. Chem. Phys.*, 1996, **105**, 10332-10348.

21 G. M. Chaban, J. O. Jung and R. B. Gerber, *J. Chem. Phys.*, 1999, **111**, 1823-1829.

22 G. M. Chaban, J. O. Jung and R. B. Gerber, *J. Phys. Chem. A*, 2000, **104**, 2772-2279.

23 J. O. Jung and R. B. Gerber, *J. Chem. Phys.*, 1996, **105**, 10682-10690.

24 M. Valiev, E. J. Bylaska, N. Govind, K. Kowalski, T. P. Straatsma, H. J. J. van Dam, D. Wang, J. Nieplocha, E. Apra, T. L. Windus, W. A. de Jong, *Comput. Phys. Commu*., 2010, **181**, 1477-1489.

25 R. F. W. Bader, 22nd International Series of Monographs on Chemistry, Oxford University Press, Oxford, U.K., 1990.

26 B. Silvi and A. Savin, *Nature*, 1994, **371**, 683-686.

27 T. Lu and F. Chen, *J. Comp. Chem.*, 2012, **33**, 580-592.

28 C. Ó. C. Jiménez-Halla, I. Fernández and G. Frenking, *Angew. Chem. Int. Ed.*, 2009, **48**, 366-369.

29 A. Bondi. *J. Phys. Chem.*, 1964, **68**, 441-451.

30 A. Lignell, L. Khriachtchev, J. Lundell, H. Tanskanen and M. Räsänen, *J. Chem. Phys*., 2006, **125**, 184514.

31 I. Fernández and G. Frenking, *Phys. Chem. Chem. Phys*. 2012, **14**, 14869-14877.

32 Y. L. Liu, Y. H. Chang, T. H. Li, H. R. Chen and W. P. Hu, *Chem. Phys. Lett*., 2007, **439**, 14-17.

33 S. A. Cooke and M. C. L. Geery, *J. Am. Chem. Soc.*, 2004, **126**, 17000-17008.

34 J. M. Michaud, S. A. Cooke and M. C. L. Gerry, *Inorg. Chem.*, 2004, **43**, 3871-3881.

35 J. M. Thomas, N. R. Walker, S. A. Cooke and M. C. Gerry, *J. Am. Chem. Soc.*, 2004, **126**, 1235-1246.

36 B. Cordero, V. Gómez, A. E. Platero-Prats, M. Revés, J. Echeverría, E. Cremades and S. Alvarez, *Dalton Trans.*, 2008, 2832-2838.

37 S. Alvarez, *Dalton Trans*., 2013, **42**, 8617-8636.

38 J. Vogt and S. Alvarez, *Inorg. Chem.*, 2014, **53**, 9260-9266.

39 L. Pauling, *J. Am. Chem. Soc.* 1927, **49**, 765-790.

40 P. Pyykkö and M. Atsumi, *Chem.-Eur. J.*, 2009, **15**, 186-197.

41 W. Zou, D. Nori-Shargh and J. E. Boggs, *J. Phys. Chem. A*, 2012, **117**, 207-212.

42 R. J. Gillespie, *J. Chem. Educ.* 1963, **40**, 295.

43 A. Sirohiwal, D. Manna, A. Ghosh, T. Jayasekharan and T. K. Ghanty, *J. Phys. Chem. A*, 2013, **117**, 10772-10782.

44 L. Pauling, *The Nature of the Chemical Bond*. Vol. 3, Cornell university press. Ithaca, NY, 1960, pp. 175.

45 M. Pettersson, L. Khriachtchev, A. Lignell, M. Räsänen and R. B. Gerber, *J. Chem. Phys*. 2002, **116**, 2508-2515.

**Table 1** Optimized geometrical parameters of $F_2BNgF$ ($C_{2v}$), $FBNg_2F_2$ ($C_{2v}$) and $BNg_3F_3$ ($D_{3h}$) (Ng=Ar, Kr, Xe) at the M06-2X, MP2, CCSD(T) and CASSCF levels, respectively. Note that bond lengths are in Å and angles in degrees.

| | | $F_2BArF$ | | | $F_2BKrF$ | | | $F_2BXeF$[b] | |
|---|---|---|---|---|---|---|---|---|---|
| methods | L(Ng-B) | L(Ng-F) | L(Ng-Ng) | L(Ng-B) | L(Ng-F) | L(Ng-Ng) | L(Ng-B) | L(Ng-F) | L(Ng-Ng) |
| M06-2X | 1.841 | 2.082 | | 2.008 | 2.096 | | 2.222/*2.212*/**2.218** | 2.148/*2.150*/**2.137** | |
| MP2 | 1.835 | 2.075 | | 1.991 | 2.098 | | 2.203/*2.196*/**2.180** | 2.172/*2.158*/**2.149** | |
| MP2[a] | 1.853 | 2.089 | | 1.994 | 2.104 | | 2.435 | 2.186 | |
| | | $FBAr_2F_2$ | | | $FBKr_2F_2$ | | | $FBXe_2F_2$ | |
| M06-2X | 1.846 | 2.000 | 3.199 | 2.016 | 2.059 | 3.523 | 2.239/*2.228*/**2.231** | 2.134/*2.135*/**2.128** | 3.857/*3.852*/**3.089** |
| MP2 | 1.863 | 1.991 | 3.203 | 2.009 | 2.052 | 3.482 | 2.221/*2.212*/**2.198** | 2.153/*2.140*/**2.136** | 3.881/*3.867*/**3.873** |
| | | $BAr_3F_3$ | | | $BKr_3F_3$ | | | $BXe_3F_3$ | |
| M06-2X | 1.842 | 1.961 | 3.190 | 2.004 | 2.029 | 3.471 | 2.217/*2.208*/**2.209** | 2.118/*2.118*/**2.112** | 3.840/*3.824*/**3.826** |
| MP2 | 1.878 | 1.944 | 3.253 | 2.006 | 2.027 | 3.474 | 2.206/*2.194*/**2.188** | 2.137/*2.121*/**2.122** | 3.821/*3.800*/**3.791** |
| CCSD(T) | 1.936 | 1.998 | 3.353 | 2.027 | 2.037 | 3.511 | 2.222/**2.193** | 2.137/**2.124** | 3.849/**3.798** |
| CASSCF(18,15) | 1.796 | 1.993 | 3.111 | 1.997 | 2.049 | 3.459 | 2.264 | 2.134 | 3.921 |

[a]From ref 15, [b] values in Roman, italic and bold are corresponding to ECP of SDD, aug-cc-pVTZ-pp and LJ18 on xenon.

**Table 2.** Optimized geometrical parameters of $F_3Ng_3BF^-$(Ng=Ar, Kr, Xe) at the M06-2X and MP2 levels. Note that bond lengths are in angstroms and bond angles in degrees.

| species | methods/basis sets | L(Ng-B) | L(Ng-F) | L(Ng-Ng) | L(B-F1) | Θ(Ng-B-Ng) | Θ(Ng-B-F1) |
|---|---|---|---|---|---|---|---|
| $F_3Ar_3BF^-$ | M06-2X/aug-cc-pVTZ | 1.907 | 2.155 | 3.067 | 1.304 | 107.0 | 111.9 |
| | MP2/aug-cc-pVTZ | 1.902 | 2.147 | 3.053 | 1.314 | 106.8 | 112.0 |
| $F_3Kr_3BF^-$ | M06-2X/aug-cc-pVTZ | 2.087 | 2.212 | 3.370 | 1.319 | 107.6 | 111.3 |
| | MP2/ aug-cc-pVTZ | 2.069 | 2.199 | 3.342 | 1.332 | 107.7 | 111.2 |
| $F_3Xe_3BF^-$ | M06-2X/aug-cc-pVTZ/SDD | 2.315 | 2.274 | 3.763 | 1.335 | 108.8 | 110.1 |
| | M06-2X/aug-cc-pVTZ/LJ18 | 2.309 | 2.271 | 3.757 | 1.341 | 108.9 | 110.0 |
| | MP2/aug-cc-pVTZ/SDD | 2.294 | 2.288 | 3.727 | 1.350 | 108.6 | 110.3 |
| | MP2/aug-cc-pVTZ/LJ18 | 2.266 | 2.272 | 3.702 | 1.361 | 109.6 | 109.4 |

**Table 3.** The calculated NPA charges of $BNg_3F_3$ ($D_{3h}$) and $F_3Ng_3BF^-$ ($C_{3v}$) (Ng =Ar, Kr and Xe) at the MP2/aug-cc-pVTZ/SDD level.

| Atoms | $BAr_3F_3$ | $F_3Ar_3BF^-$ | $BKr_3F_3$ | $F_3Kr_3BF^-$ | $BXe_3F_3$ | $F_3Xe_3BF^-$ |
|---|---|---|---|---|---|---|
| *q*B | 0.641 | 0.835 | 0.245 | 0.541 | -0.267 | 0.171 |
| *q*Ng | 0.619 | 0.498 | 0.745 | 0.589 | 0.932 | 0.717 |
| *q*F | -0.832 | -0.937 | -0.826 | -0.919 | -0.844 | -0.911 |
| *q*F1[a] | | -0.518 | | -0.550 | | -0.591 |

[a]F1 atom bonded to B along with $C_3$ axis in $F_3Ng_3BF^-$.

**Table 4** The calculated relative energies (in kcal/mol) of the various dissociated species with respect to the $BNg_3F_3$ (Ng=Ar, Kr and Xe) at the CCSD(T)//M06-2X/aug-cc-pVTZ/LJ18 level with ZPVE.

| species | Ng=Ar | Ng=Kr | Ng=Xe | species | Ng=Ar | Ng=Kr | Ng=Xe |
|---|---|---|---|---|---|---|---|
| $BNg_3F_3$ | 0.00 | 0.00 | 0.00 | $BNgF(^1\Sigma)+2Ng+2F$ | -51.79 | 4.29 | 81.60 |
| TS1 | (5.70) | (13.38) | (17.99) | $BNgF(^1\Sigma)+2NgF$ | -51.55 | 3.46 | 70.94 |
| $BNg_2F_3+Ng$ | -173.42 | -145.29 | -109.50 | $BNgF(^3\Pi)+2Ng+2F$ | -46.90 | 23.89 | 115.34 |
| TS2 | -163.70 | -129.59 | -87.83 | $BNgF(^3\Pi)+2NgF$ | -46.65 | 23.20 | 104.69 |
| | (9.72) | (15.70) | (21.67) | $3F^-+B^{3+}+3Ng$ | 1370.32 | 1440.67 | 1544.57 |
| $BNgF_3+2Ng$ | -341.39 | -288.65 | -217.88 | $B^{3-}+3NgF^+$ | 1153.89 | 1116.32 | 1057.92 |
| TS3 | -334.25 | -273.62 | -192.90 | $BNg_3{}^{3+}+3F^-$ | 762.18 | 753.01 | 725.90 |
| | (7.14) | (15.03) | (24.98) | $BNg^+(^1S)+F^-+2Ng+F_2$ | 26.53 | 92.29 | 181.01 |
| $BF_3+3Ng$ | -498.79 | -427.55 | -323.47 | $BNg^+(^3P)+F^-+2Ng+F_2$ | 103.19 | 162.92 | 238.87 |
| B+3Ng+3F | -40.11 | 30.24 | 134.14 | $BNg^+(^1S)+F^-+FNgNgF$ | 103.91 | 161.36 | 212.55 |
| B+3NgF | -46.56 | 23.27 | 112.41 | $BNg^+(^3P)+F^-+FNgNgF$ | 180.57 | 230.89 | 270.40 |
| $BNg_2F_2+Ng+F$ | -27.86 | 3.39 | 53.74 | $BNg^+(^1S)+F^-+NgF_2+Ng$ | 74.95 | 107.18 | 146.57 |
| $BNg_2F_2+NgF$ | -27.74 | 3.05 | 48.42 | $BNg^+(^3P)+F^-+NgF_2+Ng$ | 151.60 | 176.72 | 204.42 |

[a]The values in parentheses are the barrier heights of corresponding transition states.

**Table 5** The calculated electron density (ρ), Laplacian electron density ($\nabla^2\rho$), energy density ($H_r$), potential energy density ($V_r$) and kinetic energy density ($G_r$) at BCP, as well as Wiberg bond indices (WBI) for $F_2BNgF$, $FBNg_2F_2$ and $BNg_3F_3$ (Ng =Ar, Kr and Xe) at the MP2/aug-cc-pVTZ/LJ18 level.

| species | bond | WBI | ρ(r) | $\nabla^2\rho(r)$ | G(r) | V(r) | G(r)/ρ(r) | -G(r)/V(r) | H(r) | type |
|---|---|---|---|---|---|---|---|---|---|---|
| $F_2BArF$ | B-Ar | 0.771 | 0.1227 | 0.0299 | 0.1198 | -0.2323 | 0.9764 | 0.5158 | -0.1124 | B,C |
| | Ar-F | 0.082 | 0.0734 | 0.3461 | 0.0922 | -0.0979 | 1.2561 | 0.9418 | -0.0057 | W[c] |
| $FBAr_2F_2$ | B-Ar | 0.802 | 0.1303 | -0.1441 | 0.0925 | -0.2210 | 0.7099 | 0.4186 | -0.1285 | A,B,C |
| | Ar-F | 0.121 | 0.0921 | 0.3762 | 0.1101 | -0.1262 | 1.1954 | 0.8724 | -0.0161 | W[c] |
| $BAr_3F_3$ | B-Ar | 0.879 | 0.1361 | -0.2426 | 0.0815 | -0.2310 | 0.5988 | 0.3528 | -0.1458 | A,B,C |
| | Ar-F | 0.147 | 0.1067 | 0.3499 | 0.1192 | -0.1509 | 1.1172 | 0.7899 | -0.0317 | W[c] |
| $F_2BKrF$ | B-Kr | 0.864 | 0.1278 | -0.2250 | 0.0705 | -0.1973 | 0.5516 | 0.3573 | -0.1268 | A,B,C |
| | Kr-F | 0.111 | 0.0812 | 0.3059 | 0.0905 | -0.1045 | 1.1145 | 0.8660 | -0.0140 | W[c] |
| $FBKr_2F$ | B-Kr | 0.893 | 0.1316 | -0.3206 | 0.0467 | -0.1735 | 0.3549 | 0.2692 | -0.1268 | A,B,C |
| | Kr-F | 0.144 | 0.0916 | 0.3081 | 0.0986 | -0.1202 | 1.0764 | 0.8203 | -0.0216 | W[c] |
| $BKr_3F_3$ | B-Kr | 0.945 | 0.1355 | -0.3474 | 0.0379 | -0.1626 | 0.2797 | 0.2331 | -0.1247 | A,B,C |
| | Kr-F | 0.166 | 0.0980 | 0.3052 | 0.1032 | -0.1300 | 1.0531 | 0.7938 | -0.0269 | W[c] |
| $F_2BXeF$ | B-Xe | 0.956 | 0.1295 | -0.2679 | 0.0207 | -0.1083 | 0.1598 | 0.1911 | -0.0887 | A,B,C |
| | Xe-F | 0.123 | 0.0856 | 0.2829 | 0.0896 | -0.1085 | 1.0467 | 0.8258 | -0.0243 | W[c] |
| $FBXe_2F_2$ | B-Xe | 0.987 | 0.1254 | -0.2194 | 0.0231 | -0.1010 | 0.1842 | 0.2287 | -0.0792 | A,B,C |
| | Xe-F | 0.152 | 0.0886 | 0.2834 | 0.0916 | -0.1123 | 1.0339 | 0.8157 | -0.0267 | W[c] |
| $BXe_3F_3$ | B-Xe | 1.037 | 0.1263 | -0.1999 | 0.0263 | -0.1027 | 0.2082 | 0.2561 | -0.0777 | A,B,C |
| | Xe-F | 0.168 | 0.0915 | 0.2878 | 0.0942 | -0.1164 | 1.0295 | 0.8093 | -0.0290 | W[c] |

**Table 6** The calculated harmonic vibrational frequencies ($cm^{-1}$) and intensities (km/mol) of $BNg_3F_3$ (Ng=Ar, Kr and Xe) ($D_{3h}$) minima at the MP2 and M06-2X levels with aug-cc-pVTZ/LJ18 basis set, and MP2/CC-VSCF calculated anharmonic frequencies.

| normal modes | | Ng=Ar | | | Ng=Kr | | | Ng=Xe | | |
|---|---|---|---|---|---|---|---|---|---|---|
| | S-D[a] | MP2 | CC-VSCF | M06-2X | MP2 | CC-VSCF | M06-2X | MP2 | CC-VSCF | M06-2X |
| δ(Ng-B-Ng) | $E^{'}$-2 | 62.7(26) | 54.1(8) | 68.0(21) | 51.2(14) | 60.1(18) | 42.0(15) | 48.6(9) | 54.8(12) | 40.7(9) |
| Ng-B-Ng-F torsion | $A_2^{''}$-1 | 55.7(84) | 45.2(85) | 82.0(71) | 47.2(48) | 64.7(70) | 46.6(53) | 54.3(41) | 67.4(53) | 56.5(40) |
| Ng-B-Ng-F torsion | $E^{''}$-2 | 132.1(0) | 141.9(0) | 144.3(0) | 107.9(0) | 123.9(0) | 106.0(0) | 97.4(0) | 111.1(0) | 106.8(0) |
| δ(B-Ng-F) | $A_2^{'}$-1 | 164.7(0) | 165.0(0) | 174.2(0) | 135.1(0) | 139.3(0) | 125.3(0) | 121.1(0) | 126.3(0) | 119.5(0) |
| $\nu_s$(B-Ng) | $A^{'}$-1 | 228.9(0) | 310.4(0) | 204.2(0) | 156.5(0) | 206.2(0) | 168.3(0) | 145.0(0) | 148.0(0) | 141.7(0) |
| δ(B-Ng-F) | $E^{'}$-2 | 248.5(0) | 232(2) | 240.2(2) | 179.0(1) | 183.2(5) | 176.0(2) | 156.6(6) | 156.4(0) | 154.2(6) |
| $\nu_{as}$(Ng-F) | $E^{'}$-2 | 445.0(795) | 435.2(896) | 457.7(621) | 442.2(565) | 394.0(732) | 418.1(566) | 439.8(518) | 382.5(671) | 435.2(560) |
| Ng-Ng-Ng-B out[b] | $A_2^{''}$-1 | 514.4(8) | 525.0(9) | 476.6(3) | 459.8(1) | 483.7(3) | 448.6(1) | 441.1(6) | 431.9(0) | 420.9(4) |
| $\nu_s$(Ng-F) | $A_1^{'}$-1 | 547.5(0) | 497.6(0) | 552.1(0) | 495.0(0) | 465.9(0) | 479.1(0) | 476.2(0) | 458.6(0) | 479.1(0) |
| $\nu_{as}$(B-Ng) | $E^{'}$-2 | 775.0(6) | 693.5(2) | 729.0(16) | 672.8(2) | 701.4(8) | 695.7(1) | 678.2(1) | 677.2(7) | 668.2(6) |

[a] S-D represents Symmetry-Degeneracy, [b] out-of-plane torsion mode.

Figure Captions

**Figure 1** Rational frames of geometrical structures.

**Figure 2** The schematic potential energy surface (PES) of $BNg_3F_3$ dissociated to $BF_3$+3Ng (Ng=Ar, Kr and Xe).

**Figure 3** Contour line diagrams showing the Laplacian electron density, $\nabla^2\rho$, for $F_2BNgF$ (a-c), $FBNg_2F_2$ (d-f) and $BNg_3F_3$ (g-i) (Ng=Ar, Kr and Xe) calculated at the MP2/aug-cc-pVTZ/SDD level. The green lines indicate regions of charge depletion ($\nabla^2\rho>0$), and bule lines indicate regions of charge concentration ($\nabla^2\rho<0$). Bond critical points (BCP) (3,-1) are shown in blue and nuclear critical points (NCP) (3,-3) in brown. Red lines connecting critical points are the bond paths, and the black lines crossing the bond paths indicate the zero-flux surfaces in the molecular plane.

**Figure 4** Color-scale plot of the electron localization function (ELF) for $BNg_3F_3$ (Ng=Ar, Kr and Xe) at the MP2/aug-cc-pVTZ/pp level.

**Fig.1**

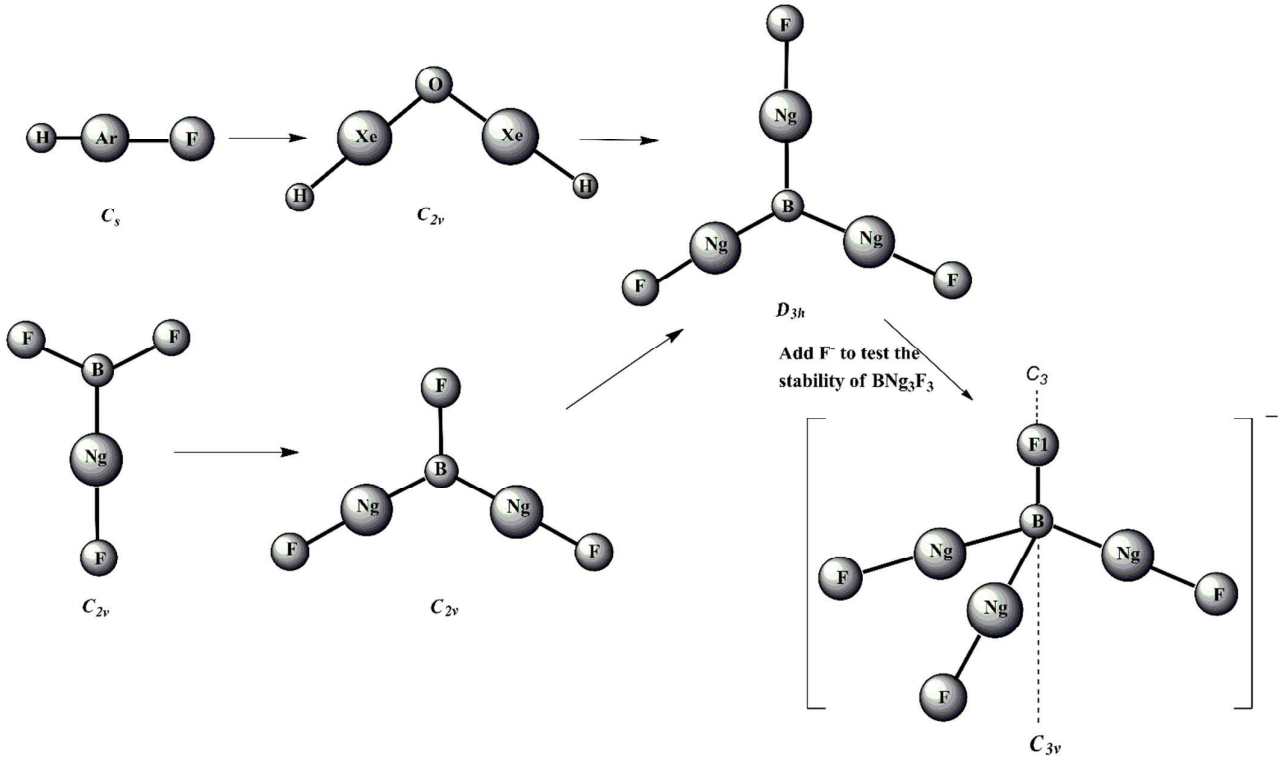

**Fig. 2**

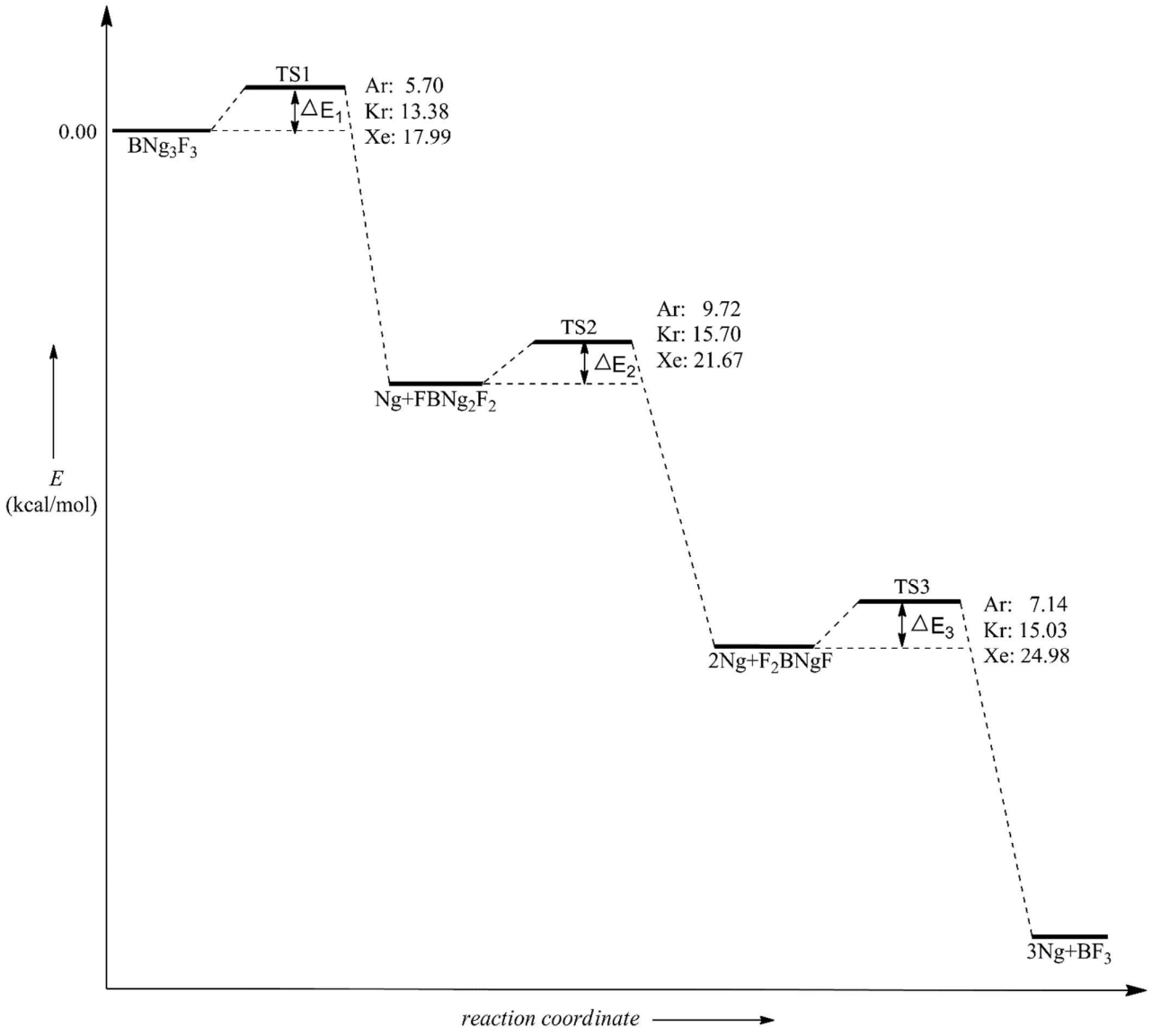

**Fig. 3**

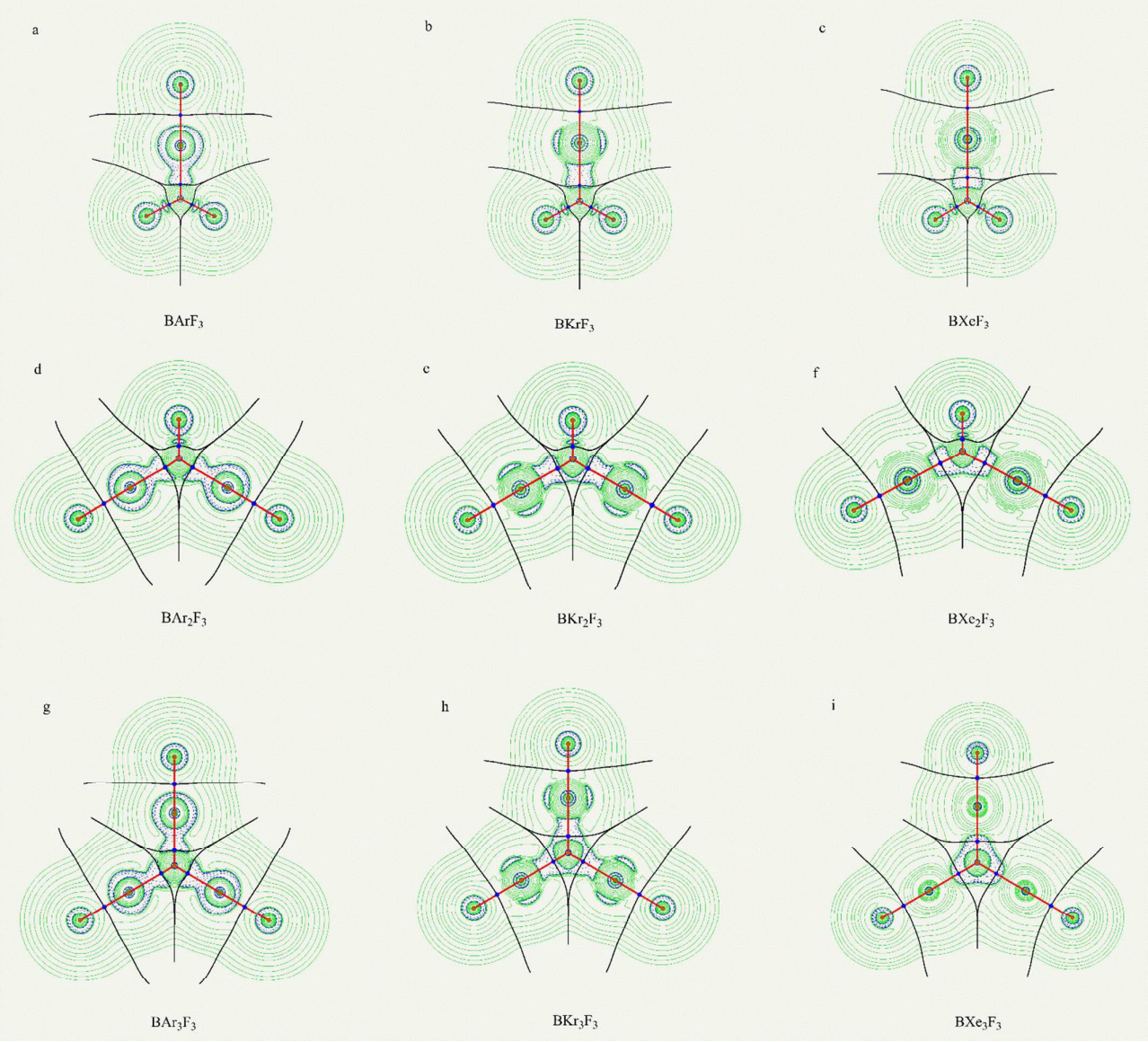

**Fig. 4**

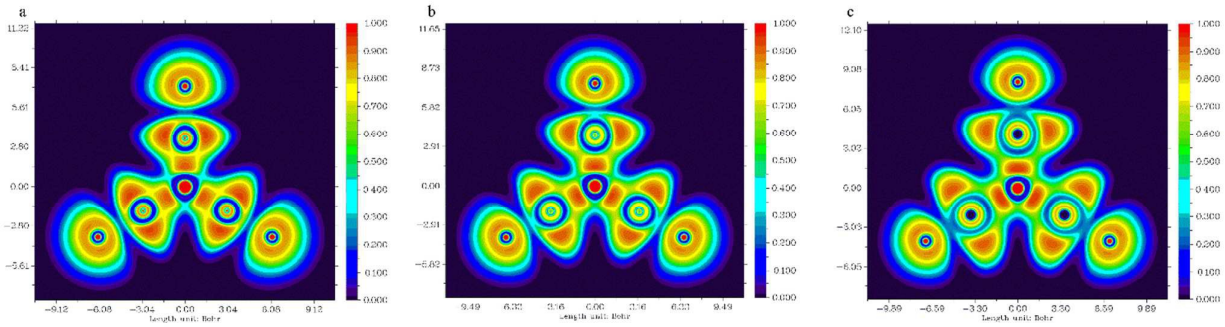

Table of Content

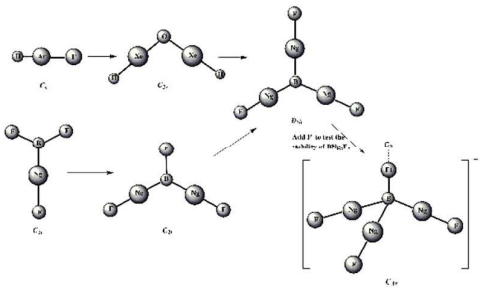

***KEYWORDS*** *quantum chemistry calculations • boron trifluoride • insertion • noble gases • Mono-centric*